# Piling and avalanches of magnetized particles

S. Fazekas,[1,2] J. Kertész,[1] and D. E. Wolf[3]
[1]*Department of Theoretical Physics, Budapest University of Technology and Economics', H-1111 Budapest, Hungary*
[2]*Theoretical Solid State Research Group of the Hungarian Academy of Sciences, Budapest University of Technology and Economics, H-1111 Budapest, Hungary*
[3]*Department of Physics, University Duisburg-Essen, D-47048 Duisburg, Germany*
(Received 9 April 2004; revised manuscript received 28 March 2005; published 22 June 2005)

We performed computer simulations based on a two-dimensional distinct element method to study granular systems of magnetized spherical particles. We measured the angle of repose and the surface roughness of particle piles, and we studied the effect of magnetization on avalanching. We report linear dependence of both angle of repose and surface roughness on the ratio $f$ of the magnetic dipole interaction and the gravitational force (*interparticle force ratio*). There is a difference in avalanche formation at small and at large interparticle force ratios. The transition is at $f_c \approx 7$. For $f < f_c$ small vertical chains follow each other at short times (*granular regime*), while for $f > f_c$ the avalanches are typically formed by one single large particle- cluster (*correlated regime*). The transition is not sharp. We give plausible estimates for $f_c$ based on stability criteria.

DOI: 10.1103/PhysRevE.71.061303 PACS number(s): 45.70.−n, 45.70.Cc, 45.70.Ht

## I. INTRODUCTION

The dipole interaction between magnetized particles can be viewed as an anisotropic adhesion force. Because its strength can be easily manipulated by the strength of the magnetizing field, magnetized particles have been recently proposed [1–3] to give insight into the transition from noncohesive to cohesive grains. Previously, adhesion effects have mainly been studied in form of moisture-induced changes, significant for industrial processes in fields such as pharmaceuticals, agriculture, and constructions.

Some time ago, Hornbaker *et al.* [4] addressed the question how sand castles stand. They stated that already small quantities of wetting liquid can dramatically change the properties of granular media, leading to large increase in the angle of repose and correlation in grain motion. Theoretical studies on the angle of repose based on stability criteria have been done by Albert *et al.* [5]. They theoretically determined the dependence of the angle of repose on cohesive forces, and applied the results to wet granular material.

Experimental studies of Tegzes *et al.* on angle of repose using the draining crater method [6] and on avalanches using a rotating drum apparatus [7] identify three distinct regimes as the liquid content is increased: a *granular regime* in which the grains move individually, a *correlated regime* in which the grains move in correlated clusters, and a *plastic regime* in which the grains flow coherently.

Experiments of Quintanilla *et al.* [8] using the rotating drum apparatus address the question of self-organized critical behavior in avalanches of slightly cohesive powders. Their results show that avalanche sizes do not follow a power-law distribution, however, they scale with powder cohesiveness. Samadani *et al.* [9] studied the effect of interstitial fluid on the angle of repose and the segregation of granular matter poured into a quasi-two-dimensional silo.

To study the transition from noncohesive to cohesive behavior, Forsyth and co-workers [1,2], adopting the widely suggested idea that competition between the interparticle forces and the inertial forces determines the behavior of cohesive granular materials, suggested a method based on magnetized particles. The particles placed in an external magnetic field become magnetized, all having the same magnetic orientation parallel to the field. Varying the strength of the field allows one to continuously vary the resulting interparticle magnetic force. Using nonmagnetic perspex walls, the particle-wall interaction remains the same as in the noncohesive state. Using particles under same packing conditions, it is ensured that the initial conditions are as uniform as possible.

Recently, Peters and Lemaire [3] extended the idea of using an external magnetic field to control the cohesiveness of the particles to rotating fields. They argue that a rotating field solves the problem of the high anisotropy introduced by the fixed external field used in the experiments of Forsyth and co-workers [1,2].

We carried out computer simulations on a system corresponding to the experiments of Forsyth co-workers [1,2] and studied the angle of repose, the surface roughness, and the effect of magnetization on avalanching in two-dimensional particle piles.

The magnetic interaction of magnetized grains is highly anisotropic, and the fixed external field introduces even more anisotropy as the grains are aligned to the field. A similar experimental setup [10], but with particles carrying a remanent magnetization in the absence of an external magnetic field, would partly diminish the mentioned anisotropy, however, in this case the magnetizations and the interparticle forces are not as well defined as in the experiments of Forsyth and co-workers [1,2]. In spite of the strong anisotropy and the longer interaction range in magnetic systems, one can expect conceptual analogies with general cohesive systems [1–3].

## II. SIMULATION METHOD

We performed computer simulations based on a two-dimensional distinct element method (DEM) [11] (for a re-

 

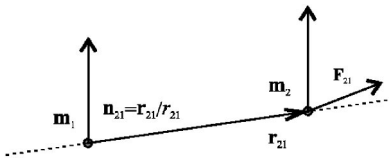


FIG. 1. Dipole-dipole arrangement. The $\mathbf{m}_1$ and $\mathbf{m}_2$ vectors denote the magnetic dipoles, $\mathbf{r}_{21}$ denotes their relative position, and $\mathbf{F}_{21}$ is the force acting on the second dipole as a result of the dipole-dipole interaction.

view see [12–14] and references therein) to study granular systems of magnetized spherical particles. The particles are magnetized by a constant external field, all having the same magnetic orientation parallel to the field. The magnetization is modeled with dipoles. We neglect any coupling between the magnetic orientation and particle rotation (i.e., the particles can rotate freely, while their magnetic dipole is fixed).

For characterizing the strength of the interparticle force, we introduce a dimensionless quantity defined by the ratio of the maximum magnetic interparticle force at contact and the gravitational force.

The magnetic force acting on a dipole $\mathbf{m}_2$ situated at distance $r_{21}$ from a dipole $\mathbf{m}_1$, along the direction $\mathbf{n}_{21}=\mathbf{r}_{21}/r_{21}$ oriented from 1 toward 2 (see Fig. 1) is given by

$$\mathbf{F}_{21}=\frac{\mu_0}{4\pi}\frac{3}{r_{21}^4}[(\mathbf{n}_{21}\mathbf{m}_2)\mathbf{m}_1+(\mathbf{n}_{21}\mathbf{m}_1)\mathbf{m}_2-5(\mathbf{n}_{21}\mathbf{m}_1)(\mathbf{n}_{21}\mathbf{m}_2)\mathbf{n}_{21}+(\mathbf{m}_1\mathbf{m}_2)\mathbf{n}_{21}]. \quad (1)$$

For identical hard spherical particles of diameter $D$ and magnetic dipole $S$, the largest possible dipole-dipole magnetic force is

$$F_m=\frac{\mu_0}{4\pi}\frac{6S^2}{D^4}, \quad (2)$$

which corresponds to a head-to-tail configuration, the dipoles having the same orientation.

We note here that the head-to-tail configuration is the energetically most favorable configuration, and consequently, dipolar spheres due to dipole-dipole interactions tend to aggregate into chain-like structures (see, for example, [15,16] and references therein) in which the energies of intrachain interactions are much greater than those of interchain interactions.

We define the magnetic *interparticle force ratio* as

$$f=F_m/F_g, \quad (3)$$

where $F_g=mg$ is the gravitational force ($m$ denotes the particle mass and $g$ is the gravitational acceleration).

Considering mass density $\rho$ and magnetization $M$, we have $m=\rho V$, $S=MV$, $V=\pi D^3/6$, and thus

$$f=\frac{F_m}{F_g}=\frac{\mu_0}{4\pi}\frac{6S^2}{mgD^4}=\frac{\mu_0}{4\pi}\frac{\pi M^2}{\rho gD}. \quad (4)$$

Assuming some interparticle force ratio $f$, the corresponding magnetization can be calculated from the previous equation as

$$M=\left(f\frac{4\pi}{\mu_0}\frac{\rho gD}{\pi}\right)^{1/2}. \quad (5)$$

In our simulations we used $\rho=7.5$ g/cm$^3$ (which corresponds approximately to the mass density of steel), $g=9.8$ m/s$^2$, and interparticle force ratio $f\leqslant 24$.

The diameter of the spherical particles was taken from the 0.7–0.9 mm interval, with a Gauss-like distribution having the mean of 0.8 mm. The Gauss-like distribution is given by the average of four independent uniformly distributed random variables in the mentioned interval. This is nearly a Gaussian distribution with $\sigma=29.8$ $\mu$m standard deviation cut at $3.35\sigma$ around the mean value. This polydispersity, resembling real experimental setups, is used to avoid effects originating from symmetries of monodisperse systems. This system is polydisperse enough that crystalline order is avoided in the absence of magnetic field. However, the magnetic interaction favors a triangular lattice with ferromagnetic ordering.

The long-range magnetic interaction is taken in consideration within a reasonable cutoff distance as a dipole-dipole interaction. We choose the magnetic interaction cutoff at $6.25D$ (where $D$ is the average particle diameter). As shown in a previous study [17], a value $5D$ already gives a reasonable magnetic interaction cutoff in two-dimensional dipolar hard sphere systems regarding the local ordering. The angle of repose, the surface roughness, and the particle avalanches depend crucially on local ordering inside the pile, as noted for example by Altshuler *et al.* [18]. The used cutoff keeps the character of local orderings and changes the magnetic energy per particle by less than 5% [17].

We can further explain the choice of the interaction cutoff distance with the fact that the strongest magnetization considered in this investigation corresponds to $f=24$. Even in this case, the magnetic interaction beyond our cutoff is negligible as compared to the gravitational as well as short range magnetic contributions. The magnetic interaction is the largest if the particle centers are on the magnetic field axis. The interaction force at the cutoff distance (i.e., $r_{21}=6.25D$) is only $1/1525$ times the force at contact position. If we change the direction of their relative position ($\mathbf{n}_{21}$), then we have even smaller forces. This means that the magnetic forces originated from the grains outside the cutoff distance are at least 3 orders of magnitude smaller than the first-neighbor magnetic interaction forces. At the same time these forces are still smaller than the gravitational force by a factor of at least $24/1525$. Therefore, it is reasonable to neglect these forces.

We calculate the collision interaction of particles using the Hertz contact model [19] with appropriate damping [20,21]. We implement Coulomb sliding friction for large relative translational velocities and for numerical stability viscous friction for small velocities, with continuous transition between the two, controlled by $\lambda=10$ kg/s viscous friction coefficient (see Fig. 2). The value of $\lambda$ was chosen such that viscous friction plays a role only up to velocities in the order of magnitude of the velocity gained by a particle in free fall during one simulation time step. We do not use any static or rolling friction model. A grid-based method is used to identify neighboring (and potentially colliding) particle pairs.

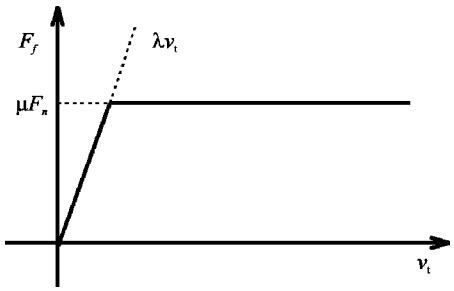


FIG. 2. The Coulomb graph of the friction model used. The frictional force $\mathbf{F}_f$ is oriented oppositely to the relative translational velocity $\mathbf{v}_t$. For large velocities, $F_f = \mu F_n$, where $\mu$ is the friction coefficient and $F_n$ is the normal force. For small velocities, $F_f = \lambda v_t$, where $\lambda$ is a large viscous friction coefficient.

The parameters of the Hertz contact model were chosen such that they correspond to a Young modulus of approximately 0.015 GPa and a restitution coefficient of approximately 0.86. These are characteristic values for hard rubber elastomers (used, for example, in constructing golf ball covers). The Young modulus is orders of magnitudes smaller than the one of steel, a choice enabling realistic CPU times with the DEM method. Nevertheless, based on our investigations, the outcome of DEM simulations (as packing, coordination number, force distribution, etc.) with the parameters we are using, are essentially those that are found in experiments.

The particle-particle and the particle-wall sliding friction coefficients were 0.5 and 0.7, respectively, (characteristic for steel-steel and steel-perspex friction).

The translational motion of particles is calculated based on Newton's equation using Verlet's leap-frog method. The rotational state of particles is integrated with Euler's method. The integration time step was 5 $\mu$s. With the elastic parameters used, a good lower estimate for collision times is 170 $\mu$s. In such conditions, the integration time step used gave good numerical stability and also fairly good response time on PCs with 1.8 GHz CPUs (available at the time of writing).

The simulation setup can be seen in Fig. 3. The external magnetic field is vertical. The particles are added one by one with constant rate along vertical trajectories at a small (maximum one particle diameter) random distance from the left wall. They either reach the pile with a given velocity (i.e., *they are fired into the pile*), or their impact velocity is set to zero (i.e., *they are placed gently on the pile*).

The system's bottom wall is sticky. Any particle touching the bottom wall sticks to it. This builds up a *random base* (see the experimental setup used by Altshuler *et al.* [18]). The particles can leave the system on the right side. The particles are removed from the simulation when their distance from the bottom-right corner is larger than the magnetic interaction cutoff distance. The width of the system is 51.25*D*. In a few cases, different sized systems were also checked and no significant changes of our results were found.

The *surface particles* (marked with black in Fig. 3) are identified with the *weighted alpha shape algorithm* [22,23]. Alpha shapes are generalizations of the convex hull and can

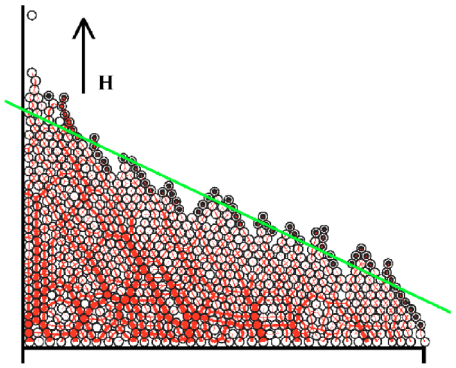


FIG. 3. (Color online) Simulation setup. The particles are introduced with constant rate one by one at small random distances from the left wall. The external magnetic field is vertical. The particles can leave the system on the right side. The angle of repose is measured by fitting a straight line over the positions of the surface particles (marked with black). The figure also shows the normal contact forces. The thickness of the lines connecting the centers of the particles in contact is proportional to the normal contact force. The sample corresponds to $f=6$ interparticle force ratio.

be used for shape reconstruction from a dense unorganized set of data points. The weighted alpha shapes are extensions of this kind of shape reconstruction to a set of spheres (as in our case). We used the implementation included in the Computational Geometry Algorithms Library [24]. The algorithm's *alpha* parameter was set to the square of the mean particle size. This gave satisfactory results. The angle of repose is measured by fitting a straight line over the positions of the surface particles. The surface roughness is given by the standard deviation of the surface points from the fitted line.

As part of our investigations, with a special *side wall model*, we also simulated the effect of front and back walls in a Hele-Shaw cell geometry encountered in experimental studies. We took into consideration the frictional interaction with side walls by summing the magnitude of normal forces acting on one particle, directing a certain percentage of this *pressure* on the walls, and deriving a frictional force using the already mentioned friction model. The percentage of the total force directed on the side walls was a parameter of our simulations.

We performed three sets of simulations: (a) the particles were fired into the pile, (b) the particles were placed gently on the pile, and (c) the particles were fired into the pile, while 4% of the internal *pressure* was directed on the *front and back walls*. In both (a) and (c), the particles reached the pile with 0.5 m/s impact velocity, which corresponds to approximately 16*D* dropping height. In all three simulation sets we executed runs at different interparticle force ratios. In each run we started with an empty system, and introducing 12 000 particles, one particle every 3000 integration steps, we numerically integrated the system for 3 min (simulated time).

In the first part of the process the number of particles in the system increased monotonically. After a pile was built, avalanches started, which in a pulsating manner moved particles out of the system. In this way, the number of particles

began to oscillate around some well-defined value. In this latter part, we identified the surface particles every 500 integration steps, and we measured the slope of the fitted surface line and the standard deviation of surface points from this line. The average of these quantities over the simulated time gave the measured angle of repose and surface roughness.

We also measured the avalanche durations and avalanche sizes. Particles are introduced at every 3000th integration step (corresponding to 15 ms). This is the smallest avalanche duration we can record. Two avalanches are separated by a "quiet" interval (time without particles leaving the system) of this length: This defines the avalanche and its duration. The number of particles leaving the system during an avalanche defines its size.

## III. SIMULATION RESULTS

### A. Angle of repose and surface roughness

In all cases, both the angle of repose and the surface roughness (in the examined domain) exhibit a linear dependence on the interparticle force ratio (see Fig. 4).

The angle of repose in cases (a) and (b) increases by approximately 0.5 degrees per unit change of interparticle force ratio (see upper panel in Fig. 4). This is in good accordance with the experimental results of Forsyth and coworkers [1,2], however, the angle of repose at zero magnetization in our case is about 10 degrees smaller. This can be the result of the missing side wall effect (see, for example, [25]), and the missing static and rolling friction (see, for example, [26,27]).

Recently, Peters and Lemaire [3], regarding the dependence of angle of repose on magnetization at weak magnetic fields, reported a sublinear dependence on $f$. For stronger fields, a linear relationship was found [1,2]. Our simulations are in agreement with both experimental findings: The very accurate data point at $f=0$ lies below the linear extrapolation of the data points for $f \geqslant 1$ (see upper panel of Fig. 4). This indicates that in the interval $0 \leqslant f \leqslant 1$ deviations from linearity may occur.

At zero magnetization the average surface roughness is about 0.7 particle diameters, and in all cases increases by approximately 0.12 particle diameters per unit change of interparticle force ratio (see lower panel in Fig. 4). This is again in agreement with the observations by Hutton [2] on the same experiments as described by Forsyth *et al.* [1], who found that as the field was increased the surface became more irregular.

As a consequence of our side wall model, the angle of repose in case (c) is about 8 degrees higher at zero magnetization, in agreement with experimentally observed effects of front and back walls in Hele-Shaw cells. However, the way we model the side walls leads to a stronger increase of the angle of repose with $f$ than in the experiments of Forsyth and co-workers [1,2] (see inset of upper panel in Fig. 4). The side wall effect does not influence the surface roughness (see inset of lower panel in Fig. 4).

### B. Particle avalanches at zero magnetization

We carefully examined the distribution of particle avalanches at zero magnetization in all three simulation sets. We also executed extra runs introducing a total of 144 000 particles, one particle every 3000 integration steps, integrating for a total of 36 min (simulated time). It must be noted that simulating at zero magnetization is about ten times faster, because only the (short-range) collision interaction must be calculated. This permitted longer simulation times. The corresponding particle avalanche size and duration statistics can be seen in Fig. 5.

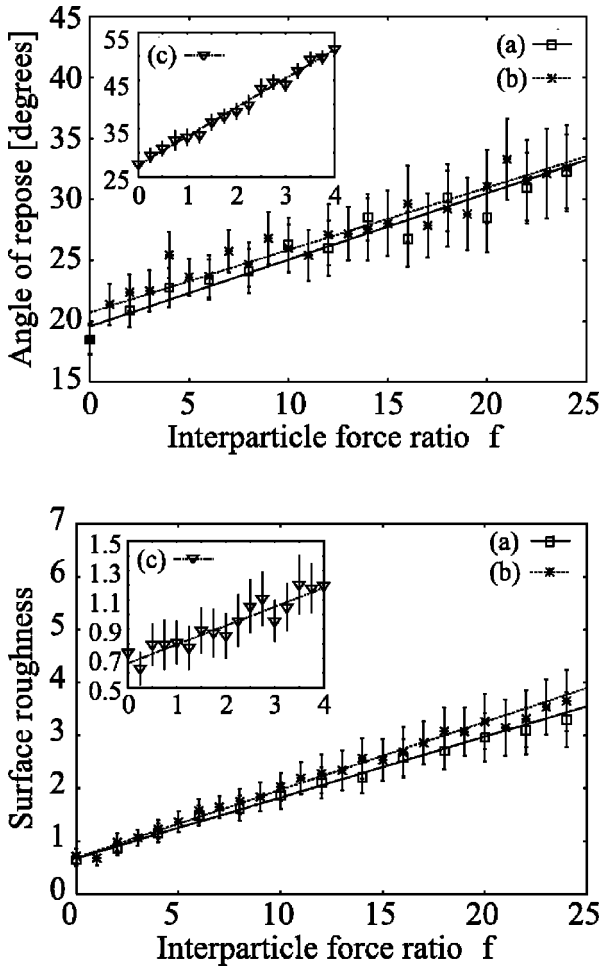


FIG. 4. Angle of repose (upper panel) and surface roughness (lower panel) at different magnetic interparticle force ratios. The angle of repose is measured in degrees. The surface roughness is measured in (average) particle diameters. We carried out three sets of simulations: In (a) and (c) the particles were fired into the pile, while in (b) the particles were placed gently on the pile. In (c) an artificial side wall effect was switched on (see text for details).

Firing the particles into the pile (i.e., dropping them from a given height) or placing them gently, and switching on or off the side wall effect gave no qualitative difference. Over both the avalanche size and duration distribution data we could fit stretched exponentials of form

$$P(x) = P_0 \exp[-(x/x_0)^{\gamma}] \tag{6}$$

with $\gamma = 0.43$.

Our $\gamma$ value is in good agreement with the experimental results of [28] and is the same value as the one found by Frette *et al.* [29] for piles of rice with small anisotropy. By

contrast, recent work of Costello *et al.* [30] presents carefully collected and detailed experimental results on piling of uniform spherical glass beads, which show a power-law behavior with an exponential cutoff. Costello *et al*. argue that the exponential cutoff depends on the height from which the particles are dropped and probably also on cohesion forces. It is clear that our simulations are different and cannot support the findings by Costello *et al.*: Most important, in our simulations the particles are introduced with a predetermined constant rate, while in the experiments a new particle was introduced only after the system is fully relaxed. Furthermore, the experiments in [30] were done in three dimensions, while our simulations are two-dimensional.

### C. Effect of magnetization on avalanches

We analyzed the effect of magnetization on particle avalanching and found that there is a difference in avalanche formation at small and at large interparticle force ratios: We identified a *granular* and a *correlated regime*. The transition between the two regimes is not sharp.

Studying the recordings from our simulations [31], it can be observed that for small magnetizations the avalanches are formed by small vertical chains following each other at short times (*granular regime*). As the particle magnetization increases beyond $f_c \approx 7$, typical avalanches consist no longer of individual chains but of one large particle-cluster with a width larger than one particle diameter (*correlated regime*). Typical examples for the two regimes are shown in Fig. 6. The avalanches are irregularly spaced in time and the larger the avalanche size, the larger the time interval between the avalanches because the steady state condition imposes an average flux of one particle per 3000 time steps.

Particles near the free surface of the pile tend to organize into clusters as a result of roughening. Such a domain of particles during avalanching may disintegrate into smaller domains or chains, or may be stable, depending on whether or not the magnetic interactions are strong enough to prevent the dilation, which is necessary to allow for relative motion of chains within the domain.

In Fig. 6, splitting can be clearly observed on the consecutive simulation snapshots taken at $f=3$ and $f=7$, while at $f=24$ a different mechanism is active. Combinations of roughening and splitting determine the size of the outflowing clusters, which typically consist of $\nu$ parallel chains of length $N$. Both $N$ and $\nu$ depend on $f$. Based on our measurements, the surface roughness increases linearly with $f$ (see Fig. 4), consequently the chain length in the outflowing clusters is proportional to $f$. In order to check to what thickness $\nu_{max}$ such a cluster is stable with respect to splitting into subclusters with fewer chains, we numerically compared the magnetic energy loss with the gravitational energy gained, when one chain is blocked while the rest of the cluster moves down by half a particle diameter (see inset of Fig. 7).

The points on Fig. 7 correspond to equal magnetic energy loss and gravitational energy gain, calculated at different chain lengths $N$ and cluster widths $\nu$. Our numerical results show that the dipole-dipole interaction can only prevent cluster splitting, if the cluster consists of less than $\nu \approx 1+f/6$ chains. This means that a cluster of two chains can be stable only for $f > f_c \approx 6$. Below this value one expects strong splitting.

This argument is certainly oversimplified: If one would take it literally, one would conclude that there should be a sequence of transitions from avalanches consisting of individual chains to those of chain pairs, then to triples, and so forth. We do not find any evidence for these further transitions. Many other effects could influence the width of a large avalanche, such as crack propagation, reorientation, or buckling.

Based on the above results, we can discuss the process of avalanche formation. Already at small magnetizations the surface roughness allows for coherent motion of larger clusters up to chain length $N_{max} \propto f$. For $f < f_c \approx 6$, clusters consisting of more than one chain of particles can easily dilate and will disintegrate into isolated chains, forming a quasicontinuous flow. For $f > f_c$, clusters consisting of $\nu > 1$ chains can fall. These results are close to the observations

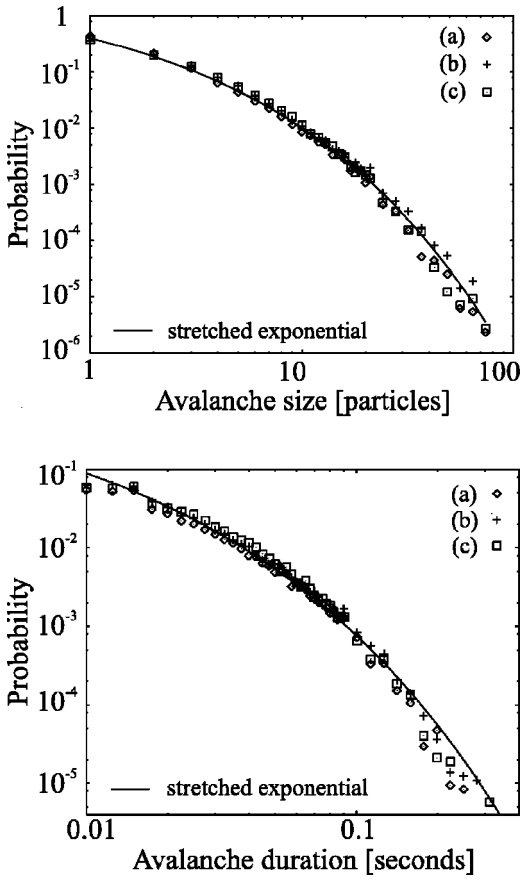


FIG. 5. Distribution of particle avalanche sizes (upper panel) and avalanche durations (lower panel) at zero magnetization. We examined three different simulation setups (see text for details). At small avalanche size and duration linear binning, at large avalanche size and duration logarithmic binning was used. Firing the particles into the pile (i.e., dropping them from a given height) or placing them gently, and switching on or off the side wall effect gave no qualitative difference. Over our simulation data (for both avalanche sizes and avalanche durations) we could fit a stretched exponential with $\gamma = 0.43$.

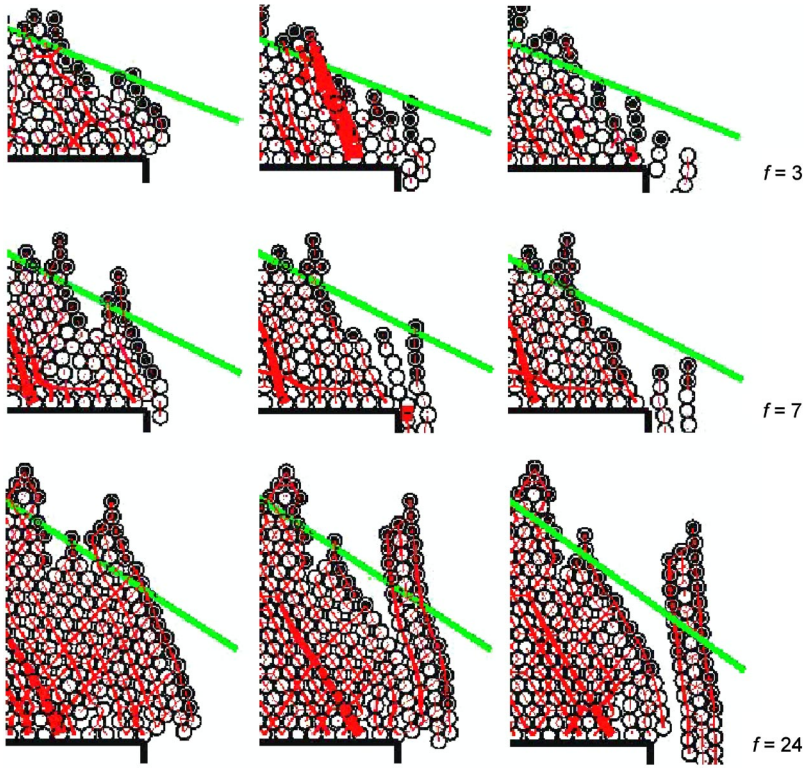


FIG. 6. (Color online) Consecutive simulation snapshots. Each row corresponds to a different value of $f$. The particles are placed gently on the pile [see the (b) simulation set]. Particles leave the system, falling at the system's boundary on the right side. Only the system's lower right corner is shown. The external magnetic field is vertical.

made on the simulations. The transition between the two regimes was observed at $f_c \approx 7$.

We show in the next subsections that the two regimes also manifest themselves in different scaling properties of avalanche sizes and durations. At given interparticle force ratios, for each avalanche size we determined the average avalanche duration (see Fig. 8). We also examined the distributions of avalanche sizes and durations.

### D. The granular regime

The avalanche size distribution at interparticle force ratios $1 < f < 7$ can be scaled together reasonably well (see Fig. 9) using the ansatz

$$P(s,f) = f^{-1} Q(s/f), \tag{7}$$

where $s$ denotes avalanche sizes, $P(s,f)$ is the probability associated with an avalanche size, and $Q(\cdot)$ is a function with integral 1 on the $[0,+\infty)$ interval.

Based on the avalanche size distributions (see Fig. 9), we argue that the magnetic cohesion introduces a well-defined characteristic size in particle avalanches. From the scaling property, we conclude that the characteristic avalanche size increases linearly with the interparticle force ratio. Qualitatively similar results were found in the experiments by Szalmás *et al.* [10].

By considering the movies of the avalanche dynamics [31] in the granular regime the following mechanism becomes apparent: The large avalanches consist of many individual chains dropping consecutively over the edge and the avalanche duration is dominated by the number $\nu$ of these chains, rather than their length $\propto f$. Therefore one expects that the avalanche duration behaves like $s/f$. In fact, we observe that the average duration of avalanches is proportional to their size (see upper panel of Fig. 8) and the proportionality factor (i.e., the slope of the lines) decreases roughly like $f^{-1}$.

### E. The correlated regime

For $f > 7$, the average duration $\tau$ of avalanches of size $s$ behaves markedly different: It is proportional to $\sqrt{s}$ and has no further $f$ dependence (see lower panel of Fig. 8). The reason is that in the correlated regime a typical avalanche duration is determined by the free fall of a large coherent cluster. Accordingly the square of the avalanche duration is proportional to the vertical extent of the cluster.

Let us assume that the width $\nu$ of the falling cluster is independent of $f$ and the height is proportional to the roughness which scales linearly with $f$. The cluster size is then $s \approx \nu f \approx f$, hence, $\tau \approx \sqrt{f}$. This is indeed verified by the data collapse shown in Fig. 10. The avalanche duration distributions $P(\tau,f)$ at interparticle force ratios $7 < f \leqslant 24$ can be scaled together reasonably well (see Fig. 10) using the ansatz

$$P(\tau,f) = f^{-1/2} Q(\tau/f^{1/2}). \tag{8}$$

A characteristic duration can be observed on Fig. 10. Based on the above scaling property, the square of the char-

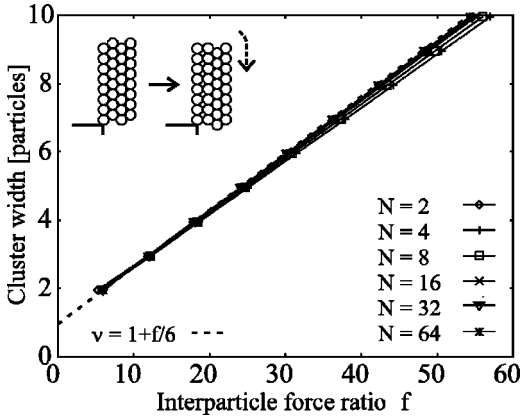


FIG. 7. Numerical results on cluster stability. At different chain lengths ($N$) and cluster widths ($\nu$) the loss in magnetic energy and the gain in gravitational energy was compared when one chain is blocked while the rest of the cluster moves down by half a particle diameter (see inset). The dashed line shows the $\nu=1+f/6$ function.

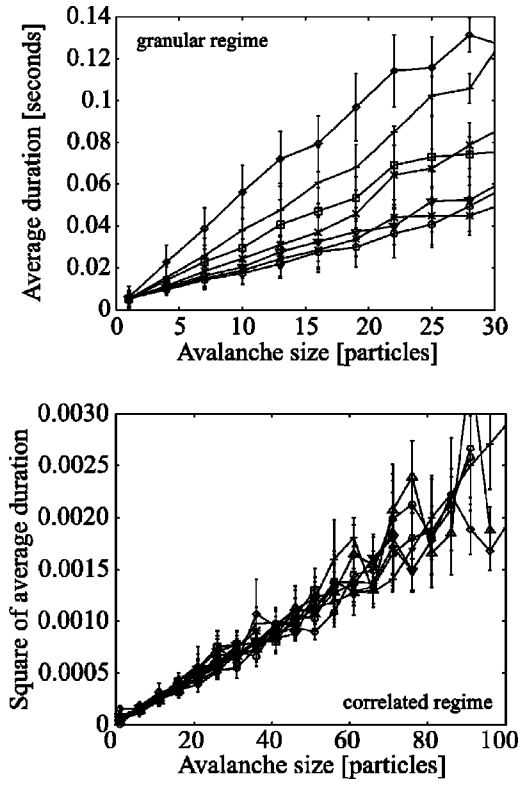


FIG. 8. Dependence of average avalanche duration on avalanche size in the (b) simulation set. The connected points correspond to equal $f$ values. The error bars show standard deviation obtained with binning. In the granular regime the average duration of avalanches is proportional to their size (see upper panel). In the correlated regime the square of the average avalanche durations is proportional to the avalanche size, with no further dependence on $f$ (see lower panel). [Similar results were found for the (a) simulation set.]

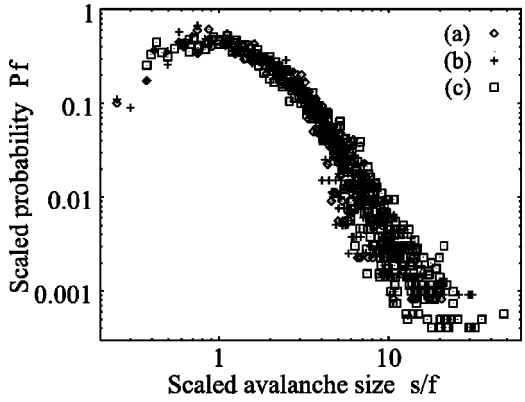


FIG. 9. Scaled avalanche size distribution in granular regime. A characteristic size can be observed. We examined three different simulation setups (see text for details). The avalanche size distribution at interparticle force ratios $1<f<7$ are scaled together using the ansatz $P(s,f)=f^{-1}Q(s/f)$, where $s$ denotes avalanche sizes. We conclude that the characteristic avalanche sizes increase linearly with $f$.

acteristic avalanche duration increases linearly with the interparticle force ratio.

## IV. CONCLUSIONS AND DISCUSSION

In this paper, we studied two-dimensional granular piles formed by magnetized particles in simulations similar to the experiments of Forsyth and co-workers [1,2]. We obtained good agreement with the experiments on the quadratic magnetization dependence of the angle of repose and the roughness of the piles. Moreover, we measured the avalanche statistics and obtained two regimes: A granular one, where the duration of the avalanches is proportional to their size, and a correlated one, where it is only proportional to the square root of their size.

We carried out computer experiments with both dropped and gently positioned particles. It turned out that in the

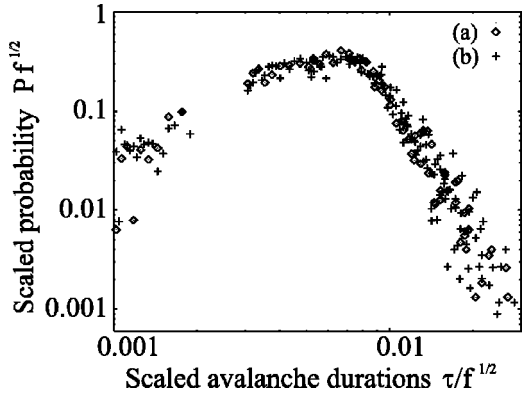


FIG. 10. Scaled avalanche duration distribution in correlated regime. A characteristic duration can be observed. We examined two simulation setups (see text for details). The avalanche duration distribution at interparticle force ratios $7<f\leqslant 24$ are scaled together using the ansatz $P(\tau,f)=f^{-1/2}Q(\tau/f^{1/2})$, where $\tau$ denotes avalanche durations. This justifies that the square of avalanche durations increase linearly with $f$.

former case the kinetic energy was weak enough so that the results were indistinguishable. We also introduced a *side wall model* simulating the effect of the front and back walls of a Hele-Shaw cell arrangement. With the parameters used, this gave no qualitatively different results in avalanche statistics, but influenced the dependence of the angle of repose on the interparticle force ratio.

We found that in the analyzed magnetization range both the angle of repose and the surface roughness exhibit linear dependence on the ratio $f$ of the maximum magnetic force at contact and the gravitational force. Because of the anisotropy of the magnetic interaction, $f$ overestimates the effective cohesion, as noticed by Forsyth and co-workers [1,2]. According to this, the angle of repose increases much more slowly with $f$ than expected from stability criteria [5] and experiments [6] on wet granular media.

The experimental results of Forsyth and co-workers and our simulations are in good accordance, although the angle of repose at zero magnetization in our case was smaller. The side wall model could increase the surface angle, but did also introduce a stronger dependence of the angle of repose on $f$ than in the experiments of Forsyth and co-workers [1,2]. Taking into consideration the static and rolling friction of particles could probably reproduce more closely the experimental results in this respect.

Tegzes *et al.* [6] found in experimental studies of wet granular media a linear dependence of the angle of repose on the liquid content in the granular regime, and an *almost* linear dependence with a slight curvature in the correlated regime. This bending could not be clearly identified in our results and most probably would require more accurate investigations at both small and large interparticle force ratios.

Tegzes *et al.* [7] reported in case of wet granular media a change in avalanche characteristics as the liquid content is increased. Based on different avalanche formation mechanisms, we could also identify a granular and a correlated regime in case of magnetized particles. The granular regime is characterized by small vertical chains following each other at short times, while in the correlated regime the avalanches are typically formed by one single large particle-cluster. The transition between the two regimes is not sharp. In simulations, we found that the transition is at $f_c \approx 7$, and we justified this with numerical calculations based on stability criteria.

In the granular regime, the average avalanche durations are proportional to avalanche sizes. We found that the ratio of avalanche size to the corresponding average duration has a linear dependence on $f$. Analyzing the avalanche size distribution, we also found that there is a characteristic size in particle avalanches. Based on the observed scaling of the avalanche size distributions with $f$, we argue that the characteristic avalanche size increases linearly with $f$.

In the correlated regime, the average avalanche durations are proportional to the square root of avalanche sizes with no further dependence on $f$. This is explained by the free fall of long particle clusters, and is justified by the scaling of the avalanche duration distributions with $f^{1/2}$. The avalanche duration distribution shows evidence of a characteristic avalanche duration proportional to the square root of the interparticle force ratio.

The results on avalanche sizes and durations may slightly depend on the chosen time scale on which the avalanches are observed, however we argue that a much coarser or finer time scale will both lead to nonphysical results, while a small correction in the time scale will not lead to a qualitative difference.

## ACKNOWLEDGMENTS

This research was carried out within the framework of the "Center for Applied Mathematics and Computational Physics" of the BUTE, and it was supported by BMBF, grant HUN 02/011, and Hungarian Grant OTKA T035028.

[1] A. J. Forsyth, S. R. Hutton, M. J. Rhodes, and C. F. Osborne, Phys. Rev. E **63**, 031302 (2001).
[2] S. Hutton, Ph.D. thesis, Monash University, 2002.
[3] F. Peters and E. Lemaire, Phys. Rev. E **69**, 061302 (2004).
[4] D. J. Hornbaker, I. Albert, A. L. Barabási, and P. Schiffer, Nature (London) **387**, 765 (1997).
[5] R. Albert, I. Albert, D. Hornbaker, P. Schiffer, and A. L. Barabási, Phys. Rev. E **56**, R6271 (1997).
[6] P. Tegzes, R. Albert, M. Paskvan, A. L. Barabási, T. Vicsek, and P. Schiffer, Phys. Rev. E **60**, 5823 (1999).
[7] P. Tegzes, T. Vicsek, and P. Schiffer, Phys. Rev. E **67**, 051303 (2003).
[8] M. A. S. Quintanilla, J. M. Valverde, A. Castellanos, and R. E. Viturro, Phys. Rev. Lett. **87**, 194301 (2001).
[9] A. Samadani and A. Kudrolli, Phys. Rev. E **64**, 051301 (2001).
[10] L. Szalmás, J. Kertész, and M. Zrínyi (unpublished); L. Szalmás, Diploma Work BUTE, 2000 [in Hungarian].
[11] P. A. Cundall and O. D. L. Strack, Geotechnique **29**, 47 (1979).
[12] G. H. Ristow, in *Annual Reviews of Computational Physics I*, edited by D. Stauffer (World Scientific, Singapore, 1994).
[13] H. J. Herrmann and S. Luding, Continuum Mech. Thermodyn. **10**, 189 (1998).
[14] S. Luding, in *The Physics of Granular Media*, edited by H. Hinrichsen and D. E. Wolf (Wiley-VCH, Weinheim, 2004).
[15] J. J. Weis, Mol. Phys. **100**, 579 (2002).
[16] W. Wen, F. Kun, K. F. Pál, D. W. Zheng, and K. N. Tu, Phys. Rev. E **59**, R4758 (1999).
[17] S. Fazekas, J. Kertész, and D. E. Wolf, Phys. Rev. E **68**, 041102 (2003).
[18] E. Altshuler, O. Ramos, C. Martinez, L. E. Flores, and C. Noda, Phys. Rev. Lett. **86**, 5490 (2001).
[19] L. D. Landau and E. M. Lifshitz, *Theory of Elasticity*, 2nd English ed. (Pergamon, New York, 1970), Chap. 9.
[20] G. Kuwabara and K. Kono, Jpn. J. Appl. Phys. **26**, 1230 (1987).
[21] N. V. Brilliantov, F. Spahn, J.-M. Hertzsch, and T. Pöschel,

Phys. Rev. E **53**, 5382 (1996).
[22] H. Edelsbrunner, Computer Science, Tech. Report UIUCDCS-R-92-1760, Univ. of Illinois, Urbana, 1992.
[23] N. Akkiraju, H. Edelsbrunner, M. Facello, P. Fu, E. P. Mucke, and C. Varela, in Proc. Internat. Comput. Geom. Software Workshop, 1995, pp. 63–66.
[24] http://www.cgal.org
[25] C. M. Dury, G. H. Ristow, J. L. Moss, and M. Nakagawa, Phys. Rev. E **57**, 4491 (1998).
[26] Y. C. Zhou, B. D. Wright, R. Y. Yang, B. H. Xu, and A. B. Yu, Physica A **269**, 536 (1999).
[27] Y. C. Zhou, B. H. Xu, A. B. Yu, and P. Zull, Powder Technol. **125**, 45 (2002).
[28] J. Feder, Fractals **3**, 431 (1995).
[29] V. Frette, K. Christensen, A. Malthe-Sorenssen, J. Feder, T. Jossang, and P. Meakin, Nature (London) **379**, 49 (1996).
[30] R. M. Costello, K. L. Cruz, C. Egnatuk, D. T. Jacobs, M. C. Krivos, T. S. Louis, R. J. Urban, and H. Wagner, Phys. Rev. E **67**, 041304 (2003).
[31] http://maxwell.phy.bme.hu/~fazekas/magaval